AN IMPROVED CHANNEL ESTIMATION ALGORITHM FOR FILTER BANK MULTICARRIER SPREAD SPECTRUM

by

Jonathan Davis Driggs

A thesis submitted to the faculty of
The University of Utah
in partial fulfillment of the requirements for the degree of

Master of Science

Department of Electrical and Computer Engineering

The University of Utah

December 2017

The University of Utah Graduate School

STATEMENT OF THESIS APPROVAL

The thesis of **Jonathan Davis Driggs**
has been approved by the following supervisory committee members:

Behrouz Farhang ,	Chair(s)	**06/14/2017** Date Approved
Rong-Rong Chen ,	Member	**06/14/2017** Date Approved
Neal Patwari ,	Member	___ Date Approved

by **Gianluca Lazzi** , Chair/Dean of
the Department/College/School of **Electrical and Computer Engineering**
and by **David B. Kieda** , Dean of The Graduate School.

ABSTRACT

Channel estimation techniques are crucial for reliable communications. This thesis is concerned with channel estimation in a filter bank multicarrier spread spectrum (FBMC-SS) system. We explore two channel estimator options: (i) a method that makes use of a periodic preamble and mimics the channel estimation techniques that are widely used in OFDM-based systems; and (ii) a method that stays within the traditional realm of filter bank signal processing. For the case where the channel noise is white, both methods are analyzed in detail and their performance is compared against their respective Cramer-Rao Lower Bounds (CRLB). Advantages and disadvantages of the two methods under different channel conditions are also discussed to provide insight to the reader as to when one will outperform the other. After the theoretical exercise of deriving these channel estimation algorithms, we examine some practical considerations for the traditional channel estimation approach such as the channel delay spread and the effects of signal interference. First, a set of guidelines about designing the subcarrier spacing of FMBC-SS vs. the channel coherence bandwidth are provided to ensure channel estimates are sufficiently unbiased. Next, we provide a method for detecting the channel delay spread and rejecting in-band interference that results in nearly unbiased channel estimation scheme that can achieve a performance close to the CRLB in low SNR environments.

CONTENTS

LIST OF FIGURES

NOTATION AND SYMBOLS

$[\mathbf{A}]_{mn}$	the element in the mth row and nth column of $\boldsymbol{A}$
$\boldsymbol{A}^{-1}$	the inverse of $\boldsymbol{A}$
$\mathbf{I}$	the identity matrix
$(\cdot)^{\mathrm{H}}$	conjugate transpose
$(\cdot)^*$	conjugate
$\boldsymbol{\mathcal{F}}$	the normalized DFT matrix, where $\boldsymbol{\mathcal{F}}\boldsymbol{\mathcal{F}}^{\mathrm{H}} = \mathbf{I}$
$x(n)$	Time indices are put in parentheses
x_n	frequency indices appear as subscripts
x_{f}	the subscript 'f' means vector carries a set of frequency domain samples
$\odot$	element-by-element vector multiplication

CHAPTER 1

INTRODUCTION

In this chapter, we introduce the FBMC-SS waveform and its benefits. Next, we discuss the channel estimation problem for FBMC and how it fits into the receiver design. Lastly, we develop a mathematical signal model for the transmitted waveform that is a foundation for the rest of the analysis presented in this thesis.

1.1 The Filter Bank Multicarrier Waveform

Filter bank multicarrier (FBMC) has been proposed as a desirable alternative to orthogonal frequency division multiplexing (OFDM) in applications where spectral efficiency and spectral mobility are important [1]. A special class of spread spectrum waveforms that are built based on FBMC (FBMC-SS) was introduced in [2]. It was noted that FBMC-SS offers robust performance in high noise and high interference applications. The robustness of the FBMC-SS can be attributed to the recombining of the spread data symbols in the receiver through the principle of maximum ratio combining (MRC), which naturally filters out those portions of the spectrum that have received a high level of interference. The combining equation requires a reasonable estimate of the communications channel. This motivates the study and development of the channel estimation algorithms presented in this thesis.

1.2 Previous Literature on Channel Estimation for Multicarrier Waveforms

The problem of estimating the channel has been well studied in OFDM literature. The presence of the cyclic prefix (CP) in OFDM introduces a periodicity in its waveform which in turn leads to a maximum likelihood (ML) channel estimator that easily achieve the Cramer-Rao lower bound (CRLB) [3]. The CP absorbs the channel transient and the samples of a single OFDM symbol (excluding the CP) contain sufficient information that

can provide an unbiased estimate of the channel impulse/frequency response. The first contribution of this thesis is to show how the channel estimation methods that have been developed for OFDM-based systems can be extended to FBMC. This method, which is examined in detail in Chapter 2, is referred to as the *OFDM-like ML channel estimator*.

In FBMC literature, most of the channel estimation methods are based on the assumption that the channel over each subcarrier band can be approximated by a flat gain [2, 4, 5]. Additional measures/steps for improving channel estimates have been explored for OFDM, e.g., the transform-domain noise reduction techniques [6–8], are also applicable and have been studied to improve the channel estimates in filter bank systems, e.g., see [9–15]. Nevertheless, some works assert that the flat-gain assumption in many cases may be too coarse and thus alternative methods such as per-subcarrier multi-tap equalization [16] have to be sought. In the second part of Chapter 2, we examine the flat-gain assumption in FBMC channel estimation and provide a detailed mathematical comparison of its performance to the approximation-free channel estimator that is obtained through the proposed OFDM-like channel estimator. We refer to this second method as *flat-gain ML channel estimator*. The results of both channel estimators are benchmarked against the CRLB. We find that while the performance of the flat-gain ML channel estimator is limited by the channel frequency selectivity, as one would expect, the proposed OFDM-like ML channel estimator remains at CRLB as the number of training symbols/pilots are increased to obtain more accurate estimates of channel.

1.3 FBMC-SS Signal Model

FBMC-SS builds its waveform using a filter bank consisting of multiple subcarriers. The case of interest in this thesis is when the same data symbol is spread across all of the subcarriers [2]. In this case, the transmitter baseband processing can be simplified to the one presented in Fig. 1.1. The transmit data symbols are up-sampled by a factor of L and passed through a synthesis filter bank $g(n)$ with N active subcarriers; see [2] for details. Accordingly, the synthesized transmit signal can be expressed as

$$x(n) = \sum_{m} s(m)g(n - mL) \tag{1.1}$$

where $s(m)$ are data symbols. At the beginning of each data packet, $s(m)$ is replaced by a sequence of training/pilot symbols, $a(m)$, that will be used for packet detection, timing

recovery, and channel estimation. Packet detection and timing recovery are performed separately and prior to channel estimation. A method for performing these tasks is discussed in [17] and [18].

In this thesis, we assume $a(m)$ is a periodic sequence with a period of K symbols. When this sequence is sent through the FBMC-SS transmitter, the result, after passing through its transient period, will be a sequence with a period of KL samples. We use $\tilde{x}(n)$ when reference is made to this periodic sequence. Periodicity of $\tilde{x}(n)$ implies that it is a summation of KL complex sine waves with frequencies $f_k = \frac{2\pi k}{KL}$ for $k = 0, 1, \cdots, KL-1$, i.e.,

$$\tilde{x}(n) = \frac{1}{\sqrt{KL}} \sum_{k=0}^{KL-1} \widetilde{X}_k e^{j\frac{2\pi kn}{KL}} \tag{1.2}$$

where $\widetilde{X}_k$ are the Fourier series coefficients of $\tilde{x}(n)$.

The derivations in the next chapter will be greatly simplified through use of a set of vectors and matrices. With this in mind, we define the column vectors $\mathbf{x} = [\tilde{x}(0)\ \tilde{x}(1)\ \cdots\ \tilde{x}(KL-1)]^T$ and $\mathbf{x}_\mathrm{f} = \left[\widetilde{X}_0\ \widetilde{X}_1\ \cdots\ \widetilde{X}_{KL-1}\right]^T$.

The terms $\mathbf{x}$ and $\mathbf{x}_\mathrm{f}$ are related according to the equation

$$\mathbf{x}_\mathrm{f} = \boldsymbol{\mathcal{F}}\mathbf{x}. \tag{1.3}$$

Also, to facilitate some of our derivations in the rest of the thesis, we define

$$\mathbf{X}_\mathrm{f} = \mathrm{diag}\left(\mathbf{x}_\mathrm{f}\right) \tag{1.4}$$

where $\mathrm{diag}(\cdot)$ refers to forming a diagonal matrix with the indicated elements.

The rest of the thesis will be organized as follows. In Chapter 2, we derive the flat-gain ML channel estimator and OFDM-like ML channel estimator. The performance of both ML algorithms is analyzed in terms of MSE, and the theoretical MSE expressions for the estimators are compared to the Cramer-Rao Lower Bound. Simulation results are provided to confirm the analysis for the channel estimation algorithms. In Chapter 3, we examine the flat-gain assumption and discuss the effects of interference and the channel delay spread on the performance of the flat-gain ML channel estimator. An approach for removing interference from the channel estimate and detecting the channel delay spread is presented that allows the estimator to achieve good performance in realistic environments. Lastly, conclusions of the thesis are presented in Chapter 4. The results in Chapter 2 were presented

at IEEE ICC 2017 [19]. Also, the combination of Chapters 2 and 3 will be combined into a journal paper [20].

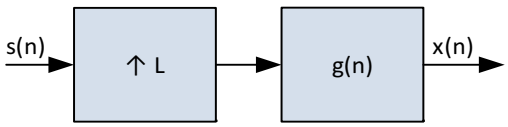

Figure 1.1. FBMC-SS transmitter model

CHAPTER 2

CHANNEL ESTIMATION

In this chapter, we present two channel estimation algorithms for the FBMC-SS system that was introduced in Chapter 1. The first algorithm utilizes a periodic preamble sequence to create a set of tones that can be used to estimate the channel in a manner that mimics OFDM. We denote this estimator as the *OFDM-like ML channel estimator* throughout the rest of this paper. The second FBMC-SS scheme makes the assumption that the channel can be approximated as a flat-gain across each subcarrier, and these channel gains are estimated at each subcarrier after performing matched filtering. Throughout the rest of this paper, this scheme will be denoted as the *Flat-Gain ML channel estimator*. The theoretical performance of these estimation algorithms is evaluated in terms of MSE, and the MSE expressions are compared to the derived CRLB for each estimator. Simulation results are provided to confirm the analysis presented in this chapter.

2.1 OFDM-like ML Channel Estimator

After the transmitted signal passes through a channel and leaves the corresponding transient period behind, the periodic sequence $\tilde{x}(n)$ leads to a periodic received signal with the same period. The result, when expressed in the form of a Fourier series expansion, has the following form:

$$\tilde{y}(n) = \frac{1}{\sqrt{KL}} \sum_{k=0}^{KL-1} C_k \widetilde{X}_{\mathrm{k}} e^{j\frac{2\pi kn}{KL}} + v(n) \tag{2.1}$$

where C_k is the channel frequency response at frequency f_k and $v(n)$ is the channel noise. Note that $v(n)$ in general is an aperiodic sequence.

Taking a single period of $\tilde{y}(n)$ and applying a DFT to it, the result in the frequency domain may be written as

$$\mathbf{y}_{\mathrm{f}} = \mathbf{X}_{\mathrm{f}} \boldsymbol{c}_{\mathrm{f}} + \mathbf{v}_{\mathrm{f}} \tag{2.2}$$

where $\boldsymbol{c}_{\mathrm{f}}$ is a column vector with elements $C_0, C_1, \cdots, C_{KL-1}$, and definitions of $\mathbf{y}_{\mathrm{f}}$ and $\mathbf{v}_{\mathrm{f}}$

should be clear from the context. The goal here is to estimate the unknown vector $\boldsymbol{c}_{\mathrm{f}}$ from (2.2). A system model depicting the placement of the OFDM-like channel estimator in the FBMC-SS receiver is provided in Fig. 2.1.

Equation (2.2) has the familiar form of a linear model (see [21], Chapter 7). Accordingly, assuming $\mathbf{v}_{\mathrm{f}}$ has a symmetric complex Gaussian distribution with covariance matrix $\boldsymbol{\Sigma}$, (2.2) leads to the ML estimate [21]

$$\widehat{\boldsymbol{c}}_{\mathrm{f}} = \mathbf{X}_{\mathrm{f}}^{-1}\mathbf{y}_{\mathrm{f}}. \tag{2.3}$$

The above derivation implicitly assumes that the duration of the channel impulse response (in the time domain) is equal to a period of $\tilde{x}(n)$ (KL samples). Many wireless channels encountered in practice have a duration of at most 1 or 2 μs, e.g., see [22–24]. However, for the case of interest in this thesis, a period of $\tilde{x}(n)$ may be one or two orders of magnitude longer than the channel impulse response duration. Making use of this information reduces the MSE of the channel estimate by the same factor; i.e., orders of magnitude improvement in the channel estimate is possible. Such an improved channel estimate is obtained by adding the following modification to the previous formulation.

Let $\boldsymbol{c}$ be a length KL column vector denoting the time domain channel impulse response samples corresponding to the IDFT of $\boldsymbol{c}_{\mathrm{f}}$ in (2.2). If we note that only the first L_{c} samples in $\boldsymbol{c}$ contain channel information, we can denote a new column vector $\boldsymbol{c}_{\mathrm{p}}$ of length $L_{\mathrm{c}} < KL$ that only retains the channel information and discards the $KL - L_{\mathrm{c}}$ samples at the end of the vector. The frequency domain channel response $\boldsymbol{c}_{\mathrm{f}}$ can be formulated from $\boldsymbol{c}_{\mathrm{p}}$ by applying a partial DFT matrix $\boldsymbol{\mathcal{F}}_{\mathrm{p}}$ which contains the first L_{c} columns of $\boldsymbol{\mathcal{F}}$:

$$bc_{\mathrm{f}} = \boldsymbol{\mathcal{F}}_{\mathrm{p}}\boldsymbol{c}_{\mathrm{p}}. \tag{2.4}$$

By substituting (2.4) into (2.2), we get a new linear equation from which we obtain the ML estimate of $\boldsymbol{c}$ as [21]

$$\widehat{\boldsymbol{c}}_{\mathrm{D}} = ((\mathbf{X}_{\mathrm{f}}\boldsymbol{\mathcal{F}}_{\mathrm{p}})^{\mathrm{H}}\boldsymbol{\Sigma}^{-1}\mathbf{X}_{\mathrm{f}}\boldsymbol{\mathcal{F}}_{\mathrm{p}})^{-1}(\mathbf{X}_{\mathrm{f}}\boldsymbol{\mathcal{F}}_{\mathrm{p}})^{\mathbf{H}}\boldsymbol{\Sigma}^{-\mathbf{1}}\mathbf{y}_{\mathrm{f}}, \tag{2.5}$$

where the subscript D has been added to indicate that this is a 'denoised' estimate of the channel. Taking the DFT of $\widehat{\boldsymbol{c}}_{\mathrm{D}}$ leads to the improved (denoised) frequency domain estimate

$$\widehat{\boldsymbol{c}}_{\mathrm{f,D}} = \boldsymbol{\mathcal{F}}_{\mathrm{p}}\widehat{\boldsymbol{c}}_{\mathrm{D}}. \tag{2.6}$$

The complexity of the estimator given in (2.5) is discussed in Section 2.6.

2.2 Flat-Gain FBMC ML Channel Estimator

The estimator in this subsection makes the assumption that the channel frequency response is flat across each of the N frequency bands. We also assume that the combination of the transmitter pulse-shaping filter and its matched version at the receiver makes a perfect Nyquist filter. The matched filter in this case corresponds to the analysis filter bank, which has the structure defined in [2, Fig. 13]. With these assumptions and noting that the pilot subcarriers are non-overlapping, the pilot symbols will be affected by the channel gains and noise at the respective subcarriers. Note that the noise samples seen at different subcarriers are independent from one another due to the fact that the subcarrier bands are disjoint.

A system model depicting the placement of the flat-gain ML channel estimator is shown in Fig. 2.2. The matched filtered data out of the analysis filter bank's kth subcarrier can be written as

$$z_k(n) = C_k a(n) + v_k(n). \tag{2.7}$$

where $a(n)$ are the pilots symbols known to the receiver and $v_k(n)$ are the noise samples at the output of the kth subcarrier. Note that the packet detection and timing recovery block in Fig. 2.2 assures that the receiver is correctly aligned with the pilot symbols.

Because the pilot symbols in (2.7) are known to the receiver, we can multiply the received symbol by the inverse of $a(n)$ to obtain

$$z'_k(n) = C_k + v'_k(n), \tag{2.8}$$

where $v'_k(n) = v_k(n)/a(n)$ is the scaled channel noise. The use of a Nyquist filter, as well as correct timing, implies that the noise samples $v'_k(n)$ are independent and identically distributed (i.i.d.) across time n. However, it should be noted that the variance of the noise across different subcarriers need not be equal. Here, we define $\sigma^2_{v,k}$ to be the variance of the noise at subcarrier k. Additionally, we define the covariance matrix of the vector $\mathbf{v}'$ with elements $v'_0(n)$, $v'_1(n)$, $\cdots$, $v'_{N-1}(n)$ to be the diagonal matrix $\mathbf{\Lambda}$, where the kth element along its diagonal is $\sigma^2_{v,k}$.

Based on (2.8), the minimum-variance unbiased (MVUB) estimator of C_k is found to be the sample mean across the K pilot symbols [21], i.e.,

$$\widehat{C}_k = \frac{1}{K}\sum_{n=1}^{K} z'_k(n). \tag{2.9}$$

As one would expect, the variance of the MVUB estimator (2.9) decreases as the number of pilot symbols increases. The column vector $\hat{\boldsymbol{c}}_{\mathrm{f}}$ with elements $\hat{C}_0$, $\hat{C}_1$, $\cdots$, $\hat{C}_{N-1}$ is, thus, an unbiased estimate of $\boldsymbol{c}_{\mathrm{f}}$ with covariance matrix $\frac{1}{K}\boldsymbol{\Lambda}$.

The above derivations do not take into account the fact that the channel impulse response length L_{c} may be smaller than the number of frequency domain samples N. When $L_{\mathrm{c}} < N$, one may obtain an improved/denoised version of $\hat{\boldsymbol{c}}_{\mathrm{f}}$ by converting it to time domain, truncating the result to L_{c} samples, and converting back to the frequency domain. Mathematically, this can be written as

$$\widehat{\boldsymbol{c}}_{\mathrm{f,D}} = \boldsymbol{c}_{\mathrm{f}} + \boldsymbol{\mathcal{F}}\mathbf{P}_{\mathrm{c}}\boldsymbol{\mathcal{F}}^{-1}\mathbf{v}'', \tag{2.10}$$

where $\mathbf{P}_{\mathrm{c}}$ is a diagonal matrix with L_{c} ones in the first part of its diagonal and zeros in the remaining portion of the diagonal and

$$\mathbf{v}'' = \frac{1}{K}\sum_{n=1}^{K}\mathbf{v}'(n). \tag{2.11}$$

2.3 Performance Analysis

The performance of the two channel estimators can be evaluated in terms of their respective MSE. To simplify the analysis and provide more intuitive equations, we derive the MSE for each estimator under the assumption that noise introduced by the channel has a white Gaussian distribution. It will be shown that the ML estimator derived under the flat gain assumption achieves similar performance to the OFDM-like ML estimator when the flat gain assumption is accurate.

2.3.1 OFDM-like MLE Performance

To derive an expression for the OFDM-like channel estimator's MSE, we first prove that the OFDM-like ML channel estimator derived in Section 2.1 is unbiased. Starting with (2.5), and denoting $\mathbf{Z} = \boldsymbol{\mathcal{F}}_{\mathrm{p}}((\mathbf{X}_{\mathrm{f}}\boldsymbol{\mathcal{F}}_{\mathrm{p}})^{\mathbf{H}}\boldsymbol{\Sigma}^{-\mathbf{1}}\mathbf{X}_{\mathrm{f}}\boldsymbol{\mathcal{F}}_{\mathrm{p}})^{-\mathbf{1}}(\mathbf{X}_{\mathrm{f}}\boldsymbol{\mathcal{F}}_{\mathrm{p}})^{\mathbf{H}}\boldsymbol{\Sigma}^{-\mathbf{1}}$, the probability distribution of the MLE has a mean

$$E[\widehat{\mathbf{c}}_{\mathrm{f,D}}] = \mathbf{Z}\mathbf{X}_{\mathrm{f}}\boldsymbol{\mathcal{F}}_{\mathrm{p}}\mathbf{c}_{\mathrm{p}} \tag{2.12}$$

and covariance

$$\mathrm{cov}[\widehat{\mathbf{c}}_{\mathrm{f,D}}] = \mathbf{Z}\boldsymbol{\Sigma}\mathbf{Z}^{H}. \tag{2.13}$$

Simplifying the terms in (2.12) and (2.13) leads to the Gaussian PDF

$$P(\widehat{\mathbf{c}}_{\mathrm{f,D}}) \sim \mathcal{CN}\left(\boldsymbol{\mathcal{F}}_{\mathrm{p}}\mathbf{c}_{\mathrm{p}}, \mathbf{B}\right), \tag{2.14}$$

where $\mathbf{B} = \boldsymbol{\mathcal{F}}_{\mathrm{p}}((\mathbf{X}_{\mathrm{f}}\boldsymbol{\mathcal{F}}_{\mathrm{p}})^{\mathbf{H}}\boldsymbol{\Sigma}^{-\mathbf{1}}\mathbf{X}_{\mathrm{f}}\boldsymbol{\mathcal{F}}_{\mathrm{p}})^{-\mathbf{1}}\boldsymbol{\mathcal{F}}_{\mathrm{p}}^{\mathbf{H}}$. The mean of the probability density function in (2.14) is the channel frequency response. This clearly shows that the estimator is unbiased. The MSE of this unbiased estimator is expressed as

$$\mathbf{MSE} = E\left[(\widehat{\boldsymbol{c}}_{\mathrm{f}} - \boldsymbol{c}_{\mathrm{f}})^{\mathrm{H}}(\widehat{\boldsymbol{c}}_{\mathrm{f}} - \boldsymbol{c}_{\mathrm{f}})\right], \tag{2.15}$$

which is simply the sum of the diagonal elements of the estimator's covariance matrix $\mathbf{B}$. If we introduce the assumption that the additive noise is white and Gaussian where $\boldsymbol{\Sigma} = \sigma^2\mathbf{I}$, the estimator MSE is

$$\mathbf{MSE} = \sigma^2 \mathrm{tr}\left[\boldsymbol{\mathcal{F}}_{\mathrm{p}}(\boldsymbol{\mathcal{F}}_{\mathrm{p}}^{\mathrm{H}}\mathbf{X}_{\mathrm{f}}^{\mathbf{H}}\mathbf{X}_{\mathrm{f}}\boldsymbol{\mathcal{F}}_{\mathrm{p}})^{-\mathbf{1}}\boldsymbol{\mathcal{F}}_{\mathrm{p}}^{\mathbf{H}}\right] \tag{2.16}$$

where tr[·] means the trace of a matrix. As will be shown in Section 2.4.1, this theoretical mean square error corresponds to the CRLB.

2.3.2 Flat-Gain MLE Performance

In order to evaluate the performance of the flat-gain ML estimator, we first note that the estimator in (2.10) is clearly unbiased if $\mathbf{v}'$ is assumed to be zero mean. We note, however, that this is only true if the assumption of the channel being flat across each subcarrier remains accurate. When the flat gain assumption becomes less accurate, a bias ϵ will be introduced into the estimate.

The covariance of the estimator is given by

$$\mathrm{cov}\left[\widehat{\boldsymbol{c}}_{\mathrm{f,D}}\right] = \frac{1}{K}\boldsymbol{\Sigma}_{\mathrm{D}}\boldsymbol{\Lambda}\boldsymbol{\Sigma}_{\mathrm{D}}^{H}, \tag{2.17}$$

where $\boldsymbol{\Sigma}_{\mathrm{D}} = \boldsymbol{\mathcal{F}}\mathbf{P}_{\mathrm{c}}\boldsymbol{\mathcal{F}}^{-1}$. If we assume the noise is AWGN and has a variance σ^2, the covariance matrix (2.17) simplifies to $\frac{\sigma^2}{K}\boldsymbol{\Sigma}_{\mathrm{D}}$. With this simplification, and following a similar line of derivations to those in [3], we get

$$\mathbf{MSE} = \frac{\sigma^2}{K}\mathrm{tr}\left[\boldsymbol{\Sigma}_D\right] + \epsilon = \frac{L_{\mathrm{c}}\sigma^2}{K} + \epsilon. \tag{2.18}$$

2.4 Cramer-Rao Lower Bound Derivation

In this section, we derive the CRLB of both channel estimation methods and compare the results to each estimator. Throughout this section, we assume that the channel noise is white and Gaussian.

2.4.1 CRLB for the OFDM-like Formulation

In order to reduce the complexity of the derivation for the CRLB, we choose to compute the CRLB for estimating the impulse response vector $\boldsymbol{c}_{\mathrm{p}}$. To relate the CRLB for the impulse response estimate to the frequency domain estimate, we note that the efficiency of estimators is maintained over linear transformations [21, p. 37], [3].

Starting with the PDF of the receiver input data defined in (2.2), the Fisher Information Matrix $\mathbf{I}(\boldsymbol{c}_{\mathrm{p}})$ is derived as [21]

$$\begin{aligned}\mathbf{I}(\boldsymbol{c}_{\mathrm{p}}) &= -E\left[\frac{\partial^2 \ln(P(\mathbf{Y}_f;\mathbf{c}_{\mathrm{p}}))}{\partial \mathbf{c}_{\mathrm{p}} \partial {\mathbf{c}_{\mathrm{p}}}^H}\right] \\ &= \frac{1}{\sigma^2}(\mathbf{X}_{\mathrm{f}}\boldsymbol{\mathcal{F}}_{\mathrm{p}})^{\mathbf{H}}\mathbf{X}_{\mathrm{f}}\boldsymbol{\mathcal{F}}_{\mathrm{p}}. \end{aligned} \tag{2.19}$$

An estimator meets the CRLB if it satisfies the following relation between its covariance matrix and the Fisher Information Matrix [21]:

$$\boldsymbol{\Sigma}_{\widehat{\mathbf{c}}_{\mathrm{p}}} = \frac{1}{\mathbf{I}(\boldsymbol{c}_{\mathrm{p}})}. \tag{2.20}$$

In order to compute the covariance matrix of the time domain channel estimate, we begin by taking the IDFT of (2.6):

$$\widehat{\mathbf{c}}_{\mathrm{p}} = \boldsymbol{\mathcal{F}}_{\mathrm{p}}^{-1}\widehat{\boldsymbol{c}}_{\mathrm{f}}. \tag{2.21}$$

The equation in (2.21) is simply the product of a complex Gaussian vector with a linear operator. If the channel noise is assumed to be white and Gaussian, this results in the following PDF:

$$\begin{aligned} P(\widehat{\mathbf{c}}_{\mathrm{p}}, \boldsymbol{c}) &\sim \mathcal{CN}\Big(\boldsymbol{\mathcal{F}}_{\mathrm{p}}^{-1}\boldsymbol{\mathcal{F}}_{\mathrm{p}}\boldsymbol{c}_p, \\ &\qquad \sigma^2\boldsymbol{\mathcal{F}}_{\mathrm{p}}^{-1}\boldsymbol{\mathcal{F}}_{\mathrm{p}}((\mathbf{X}_{\mathrm{f}}\boldsymbol{\mathcal{F}}_{\mathrm{p}})^{\mathbf{H}}\mathbf{X}_{\mathrm{f}}\boldsymbol{\mathcal{F}}_{\mathrm{p}})^{-\mathbf{1}}\boldsymbol{\mathcal{F}}_{\mathrm{p}}^{\mathbf{H}}(\boldsymbol{\mathcal{F}}_{\mathrm{p}}^{-\mathbf{1}})^{\mathbf{H}}\Big) \\ &\sim \mathcal{CN}\Big(\boldsymbol{c}_{\mathrm{p}}, \sigma^2\big((\mathbf{X}_{\mathrm{f}}\boldsymbol{\mathcal{F}}_{\mathrm{p}})^{\mathbf{H}}\mathbf{X}_{\mathrm{f}}\boldsymbol{\mathcal{F}}_{\mathrm{p}}\big)^{-\mathbf{1}}\big)\Big). \end{aligned} \tag{2.22}$$

The covariance matrix of the channel impulse estimate in (2.22) clearly satisfies the relationship defined in (2.20). Additionally, the time domain estimator remains unbiased. Therefore, the OFDM-like channel estimator achieves the CRLB.

2.4.2 CRLB for the Flat-Gain Formulation

In this section, we show that the flat-gain ML channel estimator derived in (2.10) achieves the CRLB if the flat-gain assumption is true. In addition to performing the standard derivation for the CRLB, we note that the expression for mean square error for the flat-gain ML estimator should be conditioned by the known length of the channel impulse response L_{c}. In the time domain, this conditioning can be expressed as limiting the noise to only the samples that corrupt the impulse response samples $c(n)$ in the range $0 \leq n \leq L_{\mathrm{c}}-1$, which reduces the noise power by a factor L_{c}/N for a white noise environment. Relating this result to the frequency domain noise process, the variance of the noise at each subcarrier is also scaled by L_{c}/N. Starting by writing the conditional PDF as $p(\mathbf{z}'_{\mathrm{k}}, C_k \mid \mathrm{len}\{\boldsymbol{c}\} = L_{\mathrm{c}})$, the Fisher Information can be written as

$$\begin{aligned}\mathbf{I}(C_k) &= -E\left[\frac{\partial^2 \ln(p(\mathbf{z}'_{\mathrm{k}}, C_k \mid \mathrm{len}\{\boldsymbol{c}\} = L_{\mathrm{c}}))}{\partial C_k \partial C_k^*}\right] \\ &= -E\left[-\frac{KN}{\sigma^2 L_{\mathrm{c}}}\right] = \frac{KN}{\sigma^2 L_{\mathrm{c}}}. \end{aligned} \tag{2.23}$$

The CRLB can be written in terms of the Fisher Information as

$$\begin{aligned}\mathrm{var}(\widehat{C}_k)) &\geq \frac{1}{\mathbf{I}(C_k)} \\ &\geq \frac{\sigma^2 L_{\mathrm{c}}}{KN}, \end{aligned} \tag{2.24}$$

where K is the number of samples used in the computation of the estimate. If the error term ϵ is zero in (2.18), it can be seen that the flat-gain channel estimator meets the CRLB:

$$\frac{\sigma^2}{K}\left[\mathbf{\Sigma}_{\mathrm{D}}\right]_{\mathrm{ii}} = \left[\mathbf{I}^{-1}(\boldsymbol{c}_{\mathrm{f}})\right]_{\mathrm{ii}}. \tag{2.25}$$

2.5 Results

In this section, we provide MATLAB simulation results to confirm the theoretical work developed in the previous sections and provide intuition for practical applications. The simulation configuration is given below:

- Filter Bank Upsampling Rate $L = 128$.
- Number of Active Subcarriers $N = 64$.
- Periodic Pilot Sequence Length $K = 16$.
- The channel is static over the duration of the FBMC-SS Packet.
- Pilot symbols $a(n)$ are transmitted on all subcarriers during the preamble.
- The filter bank subcarrier spacing = 500 kHz.
- The channel length L_{c} is known *a priori* by the receiver for both estimation methods.
- White Gaussian noise is added to the channel output with the SNR swept from -10 dB Es/No to 40 dB Es/No.
- Perfect timing synchronization and carrier synchronization are assumed.
- The transient introduced by the channel is absorbed by the beginning of the preamble during packet detection such that the estimate is performed on the non-transient part of the preamble.

In order to compare the relative performance of the estimators, we compute the Normalized Mean Square Error (NMSE) of each estimator using the following equation:

$$\mathrm{NMSE} = \frac{(\widehat{\boldsymbol{c}}_{\mathrm{f}} - \boldsymbol{c}_{\mathrm{f}})^{\mathrm{H}}(\widehat{\boldsymbol{c}}_{\mathrm{f}} - \boldsymbol{c}_{\mathrm{f}})}{\boldsymbol{c}_{\mathrm{f}}^{\mathrm{H}}\boldsymbol{c}_{\mathrm{f}}}. \tag{2.26}$$

In order to quantify the measured NMSE, we proceed to normalize the theoretical expressions that met the CRLB. The theoretical MSE for the OFDM-like estimator in (2.16) is normalized according to the following equation:

$$\mathrm{NMSE}_{\mathrm{theory,OL}} = \frac{\mathrm{tr}\left[\sigma^2 \boldsymbol{\mathcal{F}}_{\mathrm{p}}(\boldsymbol{\mathcal{F}}_{\mathrm{p}}^{\mathrm{H}}\mathbf{X}_{\mathrm{f}}^{\mathbf{H}}\mathbf{X}_{\mathrm{f}}\boldsymbol{\mathcal{F}}_{\mathrm{p}})^{-\mathbf{1}}\boldsymbol{\mathcal{F}}_{\mathrm{p}}^{\mathbf{H}}\right]}{\boldsymbol{c}_{\mathrm{f}}^{\mathrm{H}}\boldsymbol{c}_{\mathrm{f}}}. \tag{2.27}$$

Additionally, the flat-gain channel estimator's theoretical MSE in (2.18) is normalized as follows:

$$\mathrm{NMSE}_{\mathrm{theory,FG}} = \frac{\mathrm{tr}\left[\frac{\sigma^2}{K}\boldsymbol{\Sigma}_D\right]}{\boldsymbol{c}_{\mathrm{f}}^{\mathrm{H}}\boldsymbol{c}_{\mathrm{f}}}. \tag{2.28}$$

The NMSE measured in simulation is compared to the normalized theoretical MSE for each estimator.

Two different channel models are used to evaluate the OFDM-like channel estimator and the flat-gain channel estimator. The first channel model used is an LTE EPA channel with a Doppler frequency of 5Hz, as defined in [22]. A snapshot of the impulse response of the LTE EPA channel is shown with its estimate in Fig. 2.3. This channel model is time-limited to approximately 500 ns, which results in a fairly wide coherence bandwidth in the frequency domain and increases the accuracy of the flat-gain assumption. The measured NMSE of the estimators and the theoretical NMSE for the estimators are shown in Fig. 2.4. It can be seen that the flat-gain channel estimator matches theory until the bias begins to dominate the NMSE at high SNR. The bias, modeled as ϵ in (2.18), is considered negligible in this scenario. Additionally, we note that the OFDM-like estimator does not suffer from any bias and matches theory across all SNR points. It is also worth noting that both theoretical NMSE curves are identical.

The second channel model used to evaluate the estimators is an LTE EVA channel with a Doppler frequency of 5Hz, as defined in [22]. We chose to use this channel model to illustrate the effectiveness of the estimators when the channel impulse response has a longer duration in time and significant frequency selectivity. In the comparison of the impulse response to the estimated impulse responses in Fig. 2.5, the bias of the flat-gain channel estimator is apparent. The stronger bias, dominated by the inaccuracy of the flat-gain assumption, is also reflected in the plot of the estimator NMSE in Fig. 2.6. These results show that the flat-gain channel estimator is a reasonable method for estimating channels with short delay spreads, but has limited performance in urban environments where the channel delay spread is larger. On the other hand, the OFDM-like channel estimator, with a proper choice of the periodic sequence length K, is very effective for estimating practical channels with a variety of delay spreads and higher frequency selectivity.

2.6 Implementation Complexity

In this section, we provide details about the practical implementation of the OFDM-like channel estimator and the flat-gain channel estimator. In both implementations, we assume that the noise introduced by the channel is white with variance σ^2. For the OFDM-like estimator, we begin with (2.6) and note that the terms $\boldsymbol{\mathcal{F}}_{\mathrm{p}}$ and $\mathbf{X}_{\mathrm{f}}$ are known by the receiver. Therefore, the ML estimate of the channel frequency response can be simplified as

$$\widehat{\boldsymbol{c}}_{\mathrm{f,D}} = \boldsymbol{\mathcal{F}}_{\mathrm{p}} \boldsymbol{\Lambda} \boldsymbol{\mathcal{F}}_{\mathrm{p}}^{H} \mathbf{X}_{\mathrm{f}}^{H} \mathbf{y}_{\mathrm{f}}. \tag{2.29}$$

The matrix $\boldsymbol{\Lambda}$ in equation (2.29) is a diagonal matrix formed by $(\boldsymbol{\mathcal{F}}_{\mathrm{p}}^{H} \mathbf{X}_{\mathrm{f}}^{H} \mathbf{X}_{\mathrm{f}} \boldsymbol{\mathcal{F}}_{\mathrm{p}})^{-1}$. It can be shown that $\boldsymbol{\Lambda}$ is diagonal due to the periodicity of the transmitted signal. Using this new notation for the channel estimate, we can compute the estimate using computationally efficient FFT and IFFT blocks as shown in Fig. 2.7. While the FFT components in Fig. 2.7 can be large, depending on KL, two of the FFTs have pruned architectures that can be implemented efficiently following the guidelines in [25, 26]. Using pruned FFT architectures, we compute the computational complexity of this estimator as $KL \log_2 KL + KL \log_2 L_{\mathrm{c}} + 3KL - L_{\mathrm{c}}$ complex multiplications and $KL \log_2 KL + KL \log_2 L_{\mathrm{c}} + 2KL - 2L_{\mathrm{c}}$ complex additions.

The flat-gain channel estimator relies on the analysis filter bank to perform matched filtering prior to the estimate, so its complexity is incorporated into this analysis. Additionally, the denoising algorithm can be implemented with a pruned FFT architecture having a complexity defined in [25]. Assuming the analysis filter bank uses a P-tap polyphase filter size and an L-point IFFT, the channel estimator described by (2.10) requires $KPL + KL \log_2 L + KN + KN (\log_2 L_{\mathrm{c}} + 2) - 2KL_{\mathrm{c}}$ complex multiplication operations and $KPL + KL \log_2 L + K^2 N + KN (\log_2 L_{\mathrm{c}} + 2) - 2KL_{\mathrm{c}} - K$ complex additions.

To compare the implementations more directly, we evaluate the estimator complexities using parameter values that are sufficient for estimating a channel similar to the LTE EPA model. For this example, we let $K = 4$, $L = 128$, $P = 6$, $N = 64$, and assume a channel impulse response duration of 0.5 μs ($L_{\mathrm{c}} = 16$). Using these parameters, the OFDM-like ML channel estimator requires 8176 complex multiplications and 7648 complex additions. On the other hand, the flat-gain ML channel estimator requires 8320 complex multiplications and 9084 complex additions. Due to the complexity of the filter bank, it is apparent that the OFDM-like ML channel estimator is a more computationally efficient algorithm.

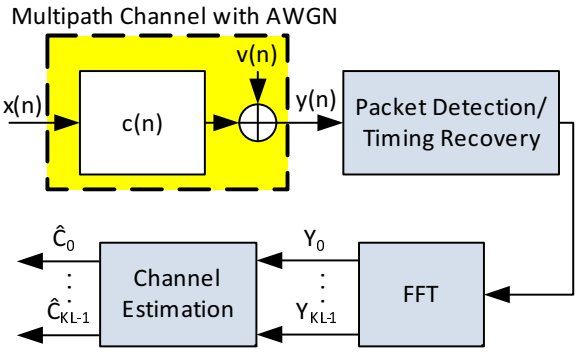

Figure 2.1. System model for the OFDM-like channel estimator

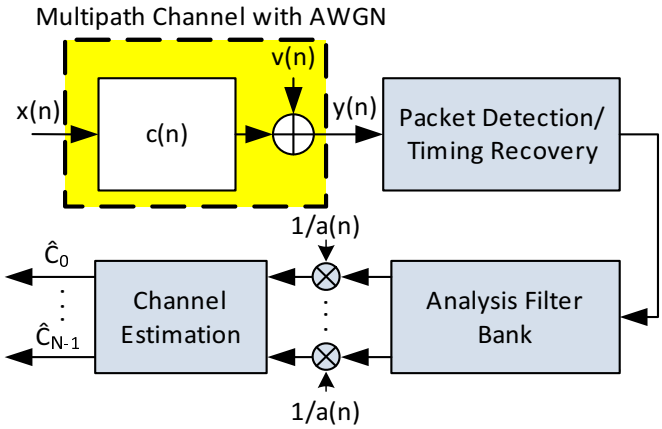

Figure 2.2. System model for the flat-gain channel estimator

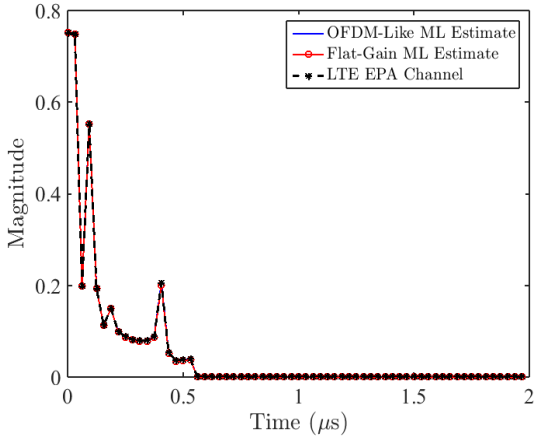

Figure 2.3. Channel impulse response estimates for the LTE EPA 5 Hz channel at High SNR

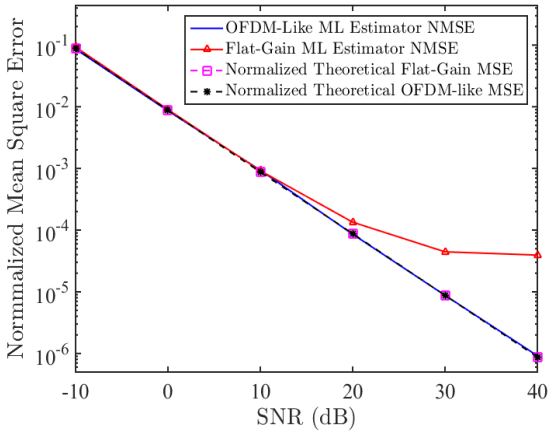

Figure 2.4. NMSE vs. received SNR for the LTE EPA 5 Hz multipath channel

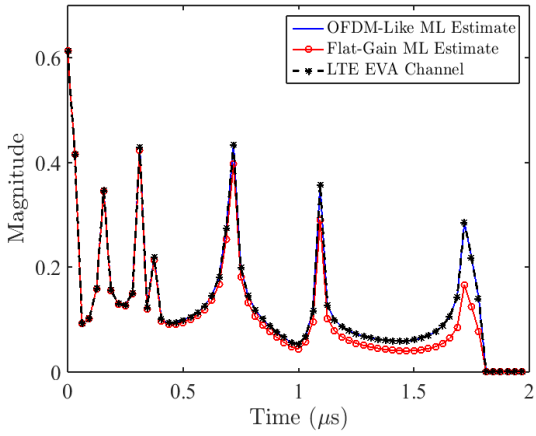

Figure 2.5. Channel impulse response estimates for the LTE EVA 5 Hz channel at High SNR

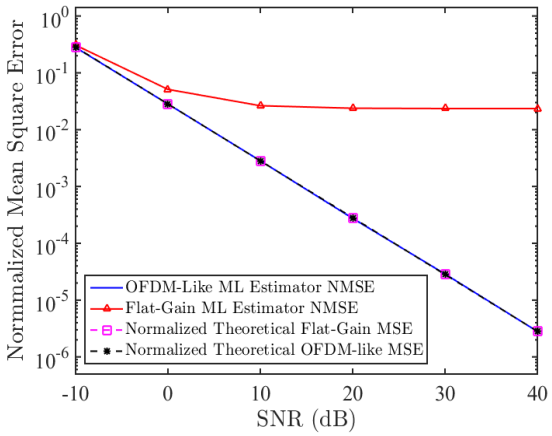

Figure 2.6. NMSE vs. received SNR for the LTE EVA 5 Hz channel

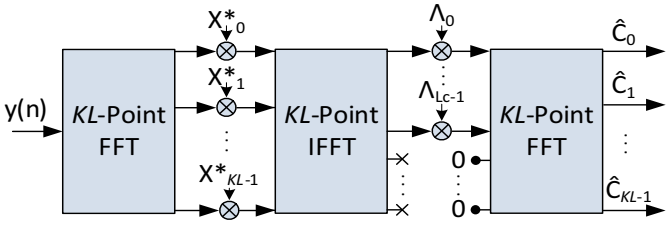

Figure 2.7. OFDM-like channel estimator implementation

CHAPTER 3

PRACTICAL IMPLEMENTATION OF THE FLAT-GAIN ML CHANNEL ESTIMATOR

In this chapter, we pursue the implementation of the Flat-gain ML Channel estimator. While the OFDM-like ML channel estimator is a more novel architecture that can achieve the CRLB for highly frequency selective channels, the high resolution of the estimate cannot be used in the current FBMC-SS receiver architecture. The FBMC-SS receiver utilizes the principle of Maximum Ratio Combining (MRC) to optimally recover data symbols. Currently, the MRC is only designed for one sample/symbol per subcarrier, rather than the K samples/subcarrier that the OFDM-like estimator provides. Therefore, we seek to determine how the flat-gain estimator can be integrated into the FBMC-SS receiver in practical scenarios.

The first analysis examines the flat-gain assumption, and when it is valid relative to the coherence bandwidth of the channel. Bit-error rate simulations are provided to support the analysis. Next, we examine the issue of interference within the received signal band, and how to handle such interference in the channel estimator. Last, we provide a method for detecting the channel impulse response delay spread in order to prevent the denoising operation from removing valid channel samples.

3.1 Flat-Gain Assumption Analysis

In Chapter 2, it was shown that the denoising ML channel estimator achieves the CRLB if the flat-gain assumption is accurate. The "flatness" of the channel frequency response corresponds to the channel coherence bandwidth, which is dependent on statistical properties of the channel. Here, we introduce a constraint that dictates when our system will perform adequately, or meet the flat-gain assumption within a good approximation, relative to statistical properties of the channel. In the thesis, we verify the constraint's accuracy through a set of BER simulations with an LTE channel model.

3.1.1 Coherence Bandwidth Constraint

The impulse response of the channel is denoted as $c(\tau, t)$ where τ is the time spread variable for the channel impulse response at the time instant t. The channel is assumed to be a wide-sense stationary uncorrelated scattering (WSSUS) Rayleigh fading channel [27]. The time variation of $c(\tau, t)$ is assumed to be slow, and may be ignored over the interval of the interest; the preamble period of each packet. We thus remove the time variable from $c(\tau, t)$ and consider the time independent channel impulse response $c(\tau)$ for the rest of our study in this chapter. Under this condition, considering the fact that the channel is WSSUS, the only statistical quantity of the channel that is of interest to us is its power delay profile, defined as

$$\rho(\tau) = E[|c(\tau)|^2]. \tag{3.1}$$

The Fourier transform of $\rho(\tau)$, that we denote by $A_\kappa(f)$, is a frequency domain function whose value at a given frequency Δf is a equal the correlation between channel frequency response samples that are at a spacing of Δf, [27]. Various definitions have appeared in the literature for the coherence bandwidth, B_c, of the channel. One common and useful definition for this thesis is

$$B_c = \frac{k}{\sigma_{\text{rms}}}, \tag{3.2}$$

where σ_{rms} is the RMS delay spread of the channel and k is a constant that may be chosen to match a case of interest, [28].

In this thesis, we let $k = 0.2$ and note that this definition defines B_c as a bandwidth over which the correlation between the channel impulse response samples (with a high probability) is greater then 0.5, [28]. That is, we define the coherence bandwidth as

$$B_{c,50\%} = \frac{k}{\sigma_{\text{rms}}}. \tag{3.3}$$

Moreover, based on our empirical results, we propose that the subcarrier bandwidth must be less than one eighth of this coherence bandwidth in order to avoid significant inter-symbol interference (ISI). This constraint can be expressed as

$$\frac{f_{\text{s}}}{L} < \frac{0.2}{8\sigma_{\text{rms}}}, \tag{3.4}$$

where f_{s} is the sampling rate. The ratio of $\dfrac{f_{\text{s}}}{L}$ is the bandwidth of a single subcarrier.

3.1.2 Simulation Results

To evaluate the validity of the constraint in (3.4), we simulate the performance of the FBMC-SS waveform with the LTE EVA channel model defined in [22]. The simulation was configured as follows:

- The Filter Bank Upsampling Rate L is varied between 128 and 512.
- The number of Active Subcarriers $N = \frac{L}{2}$.
- The channel is static over the duration of the FBMC-SS Packet.
- The channel length L_{c} is known *a priori* by the receiver, and denoising is performed according to (2.10).
- The data symbols are BPSK and there is no channel code.
- White Gaussian noise is added to the channel output with the SNR swept from E_b/N_o=4 dB to 10 dB. We note that with BPSK signaling and no channel coding, E_b/N_o is equal to SNR at the receiver input times the processing gain $2N$ of FBMC-SS.
- Perfect timing synchronization and carrier synchronization are assumed.
- The transient introduced by the channel is absorbed by the beginning of the preamble during packet detection such that the estimate is performed on the non-transient part of the preamble.

The power delay profile of the LTE EVA channel defined in [22, Table B.2.1-3] and has an RMS delay spread of 357 ns. Based on the constraint equation (3.4), the FBMC-SS subcarrier bandwidth should be less than 70 kHz:

$$\frac{f_{\mathrm{s}}}{L} < 70\,kHz. \tag{3.5}$$

If the system sampling rate is assumed to be 32.5 MHz, then the power-of-two upsampling factor L in the filter bank must be greater than or equal to 512. To validate this constriant, we provide the results of a bit-error rate simulation in Fig. 3.1.

The BER curves in Fig. 3.1 correspond to the performance of the FBMC-SS receiver with different filter bank sizes under the same conditions. From the results, it is evident that the

$L = 512$ configuration significantly outperforms the $L = 128$ and $L = 256$ configurations. The receiver with the largest subcarrier bandwidth experienced an approximately 1 dB loss in performance, while the other receiver configurations have BER performance closer to theory. It is also worth noting that the $L = 512$ configuration suffers from less performance loss than the $L = 256$ case. Beyond $L = 512$, there is about 0.1 dB gain to be made. This confirms the theoretical constraint introduced in (3.4).

3.2 Interference Detection and Rejection

The maximum-likelihood channel estimation algorithm proposed in (2.10) was derived under the assumption that the channel noise is white and Gaussian. Additionally, it was shown that the denoising operation introduces correlation between the noise samples on adjacent subcarriers in (2.17). If the input noise is correlated due to the presence of interference, the denoising operation will spread the correlated interference across all subcarriers. This distribution of interference is particularly problematic for sinusoidal narrow-band interference, where the denoising operation can distribute the interference across the subcarriers. Therefore, it is critical to detect this interference and remove it prior to denoising the channel estimate.

There are a variety of methods for detecting the presence of interference within a frequency band of interest. In cognitive radio applications, spectrum sensing is utilized to identify regions of the spectrum that are occupied by interferers [29], [30], [31]. It has also been shown that filter banks are an effective and computationally efficient spectrum sensing tool [32]. By using these spectrum sensing tools, it is possible to have *a priori* knowledge of interference locations when FBMC-SS packets are received and simply ignore interferred subcarriers in the channel estimation process. However, there are a number of complications with this spectrum sensing approach. First, the sensing algorithm needs an adequate amount of time for detection in order to meet a desired receiver operating characteristic (ROC) [33]. There are also additional practical considerations such as imperfect analog filters, finite precision A/D converters, and non-white Gaussian noise that lead to "*SNR Walls*" [34] for sensing algorithms. These considerations have motivated the development of an independent interference detection algorithm that operates on a per-packet basis.

The interference identification algorithm here utilizes the preamble sequence at the

beginning of the FBMC-SS packet. Interference is identified through a noise variance estimator, which is performed after the analysis filter bank, or at the same location as the channel estimator in Fig. 2.2. Because of the orthogonality of the individual filters in the analysis filter bank, the noise at each subcarrier can be assumed to be independent from other subcarriers. To estimate the noise variance at the k^{th} subcarrier, the noise is assumed to be white and Gaussian such that successive samples in (2.8) can be linearly combined to remove channel information and obtain

$$\beta_{\mathrm{k}}(n) = z'_{\mathrm{k}}(n) - z'_{\mathrm{k}}(n-1) = v'_{\mathrm{k}}(n) - v'_{\mathrm{k}}(n-1). \tag{3.6}$$

There are a number of assumptions made in (3.6). First, the channel is assumed to be static across the duration of the FBMC-SS packet's preamble. Additionally, we assume that any carrier offset has been compensated for such that the phase rotation between successive samples is negligible. The distribution of the expression in (3.6) is

$$P(\beta_{\mathrm{k}}) \sim \mathcal{CN}(0, 2\sigma_{\mathrm{k}}^2). \tag{3.7}$$

Neyman-Fischer factorization is used to find a sufficent statistic for the noise variance, which is simply $\frac{1}{2}\beta_{\mathrm{k}}^2$. Additionally, this statistic is the minimum variance unbiased (MVUB) estimator because (3.7) belongs to the exponential family of distributions [21], and can be written as

$$\psi_{\mathrm{k}} = \frac{1}{2K}\sum_{i=1}^{K} |\beta_{\mathrm{k}}(i)|^2. \tag{3.8}$$

The estimator in (3.8) is the sum of scaled squared standard normal random variables, which results in a scaled Chi-squared (Gamma) distribution:

$$\begin{aligned} P(\psi_{\mathrm{k}}, \alpha, \Theta) &\sim \frac{1}{|\sigma_{\mathrm{k}}^2|}\chi^2 \\ &\sim \mathbf{\Gamma}\left(\alpha = \frac{K}{2}, \Theta = \frac{2}{\sigma_{\mathrm{k}}^2}\right) = \frac{1}{\Gamma\left(\frac{K}{2}\right)\left(\frac{2}{\sigma_{\mathrm{k}}^2}\right)^K}\psi_{\mathrm{k}}^{K-1}\exp\left(-\frac{2\psi_{\mathrm{k}}}{\sigma_{\mathrm{k}}^2}\right)u(\psi_{\mathrm{k}}), \end{aligned} \tag{3.9}$$

where $u(\psi_{\mathrm{k}})$ is the unit step function and K is the preamble length. The theoretical PDF in (3.9) is shown in blue in Fig. 3.2 for a received symbol energy to noise ratio (SNR) of 0 dB and a preamble length of 32 symbols. Additionally, the distribution of the noise estimate was experimentally verified through a Monte Carlo simulation of the FBMC-SS receiver with the same SNR and preamble length and is plotted against the theoretical curve in

orange. From the results, it is evident that the noise estimate closely matches theory under the assumptions of a static channel and negligible carrier offset.

In the case of interference, the noise samples observed at each subcarrier might not be independent and identically distributed (i.i.d.) across time and the resulting distribution might not be zero mean. However, this is not a concern because any bias will drive the noise variance estimate higher and indicate the presence of interference at individual subcarriers. To detect interference, we identify subcarriers with a variance a scalar factor above the subcarrier containing the lowest noise variance estimate. Mathematically, this thresholding method can be written as

$$\begin{aligned} H_0 &: \psi_{\mathrm{k}} < a\psi_{\min} \\ H_1 &: \psi_{\mathrm{k}} \geq a\psi_{\min}, \end{aligned} \tag{3.10}$$

where a is a constant and $\psi_{\min}$ is smallest noise variance estimate.

The lowest noise estimate ($\psi_{\min}$) is assumed to be near the mean of the PDF in (3.9) due to the lower variance of the Gamma distribution. The relative interference detection threshold is coarsely set based on a desired probability of false alarm, resulting in a constant false alarm rate (CFAR) detection algorithm. Due to the inaccuracy that stems from scaling the smallest noise variance estimate sample, the scale factor a and consequent probability of false alarm should be constrained to a very low (e.g., 10^{-9}) level to minimize estimation error.

After identifying subcarriers with interference, they are zeroed and a simple linear interpolation algorithm is used to compute an approximate channel response at the gaps. An example of the interference detection algorithm output is provided in Fig. 3.3. In this simulation, a wideband signal is transmitted over approximately 20 FBMC-SS subcarriers with a signal to interference ratio of -5 dB. Additionally, the transmitted signal was convolved with a multipath channel having a RMS delay spread of 45 ns and noise was added to achieve an SNR of 0 dB. The relative detection threshold was set to five, which scaled the lowest variance measurement of 0.22 to create an interference detection threshold of 1.1. The corresponding probability of false alarm for the estimated mean of 0.22 and threshold of 1.1 is 9×10^{-4}.

3.3 Channel Delay Spread Detection

The maximum-likelihood channel estimator described in (2.6) relies on *a priori* knowledge of the channel impulse response duration in order to achieve the CRLB. In a practical system, it is difficult to assume the channel impulse response will be constrained to a specific set of samples. The main problem is that the timing recovery algorithm in the FBMC-SS receiver identifies the time index that corresponds to the peak symbol magnitude and aligns the receiver to that index. This time alignment operation also has the effect of circularly shifting the observed impulse response. In multipath environments that approach Rayleigh fading, there is no guarantee that the path with the largest power corresponds to the shortest delay. Therefore, the circular shift resulting from symbol time alignment can shift some impulse response samples with significant energy to the end of the N-sample impulse response estimate. If the denoising operation in (2.10) does not adapt to these shifts, then the truncation operation will remove valid information and bias the estimate. Here, we develop a robust detection algorithm that can identify large channel impulse response samples that have circularly shifted and adjust the denoising operation accordingly.

An example of the wrapping problem is provided in Fig. 3.4 and Fig. 3.5. A near-Rayleigh fading multipath channel without a dominant line-of-sight path is shown in Fig. 3.4. In the FBMC-SS packet detection algorithm, there is a high probability of selecting one of the many different paths that are close to the peak amplitude. If a path is picked with a larger delay, the response will shift in the receiver similar to what is shown in Fig. 3.5. Our motivation is to prevent the denoising algorithm from removing significant paths that wrap to the end of the observed response.

The problem of estimating the channel power delay profile has been studied in OFDM literature, as the channel length often has a direct effect on the computational complexity of channel estimation [7], [35]. However, few of these previous studies target low SNR scenarios where the observed channel response is near the noise floor. Several methods utilize the fact that the channel impulse response is correlated such that the cyclic correlation can be computed to identify significant paths [36], [37]. With these cyclic correlation methods, the channel length is estimated based on the position of the last detected significant path. However, these methods suffer from poor performance in low SNR conditions and high interference environments due to the corruption of the correlation result. Other promising

methods for estimating the channel length compute a statistical threshold for identifying impulse response samples above the noise floor. The work in [38] estimates the power delay profile and computes a detection threshold using the most significant sample (MSS) method, which assumes all samples in the power delay profile estimate below the mean amplitude are noise. However, the MSS thresholding method becomes increasingly biased when there are more paths in the power delay profile and with higher levels of noise. In [39], the authors derive an ML estimator that jointly estimates the multipath time delays and noise variance. Our approach in this thesis is similar to that in [39], as we jointly estimate the noise variance and channel delay spread. However, our approach does not make a central limit theorem approximation to simplify the analysis. Additionally, we choose to estimate the channel delay spread using the power delay profile, which allows us to reuse the noise variance estimate in Section. 3.2 for reduced complexity in computing a detection threshold.

In order to estimate the power delay profile in the FBMC-SS system, we leverage techniques introduced in the OFDM literature. The power delay profile (PDP) estimation technique in [40, Eq. 16] is chosen for this application. We use the PDP estimate to identify all of the significant channel response samples, rather than identifying the largest sample as in [40]. The PDP is estimated by averaging the magnitude squared of the IDFT of (2.7):

$$\widehat{\mathbf{S}} = \frac{1}{K}\sum_{n=1}^{K} \boldsymbol{\mathcal{F}}^{-1}\mathbf{z}'(n) \odot (\boldsymbol{\mathcal{F}}^{-1}\mathbf{z}'(n))^{*}. \tag{3.11}$$

The power delay profile estimate $\widehat{\mathbf{S}}$ contains N samples, and only L_{c} samples contain power delay profile samples where $L_{\mathrm{c}} < N$. Therefore, we seek to identify all samples in $\widehat{\mathbf{S}}$ that are above the noise floor with a threshold. Mathematically, this can be expressed as a hypothesis test with H_0 being the noise-only condition and H_1 being the condition where a channel impulse response sample is present:

$$\begin{aligned} H_0 &: \widehat{S}_n = \zeta \\ H_1 &: \widehat{S}_n = |c_n|^2 + \zeta. \end{aligned} \tag{3.12}$$

Additionally, we note that $\zeta = \dfrac{1}{NK}\sum_{n=1}^{K} |v'(n)|^2$ and $\widehat{S}_n$ is the power delay profile at time index n. The noise variance term ζ is normalized by the additional factor of $\dfrac{1}{N}$ due to the N-point IFFT operation.

Prior to estimation of the power delay profile, interference is rejected using the method in Section. 3.2 such that the noise process $\mathbf{v}'(n)$ in (2.7) is assumed to be a symmetric Gaussian distribution with a covariance matrix $\sigma_{\mathrm{w}}^2\mathbf{I}$. Under this assumption, the distribution of noise-only samples ζ is equivalent to the distribution of the noise estimate under the white noise condition (3.9). Utilizing this information, we form an accurate estimate of the channel noise variance by taking a mean of the noise variance estimates at different subcarriers (3.8) that do not contain interference:

$$\widehat{\sigma}_{\mathrm{w}}^2 = \frac{1}{NK_{\mathrm{n}}} \sum_{m \in K_{\mathrm{n}}} \psi_{\mathrm{m}}, \tag{3.13}$$

where $m \in K_{\mathrm{n}}$ denotes all subcarriers that contain no interference.

Using the channel noise variance estimate in (3.13), we then compute a detection threshold using the same CFAR technique in Section. 3.2. However, in this case, we have obtained a significantly more accurate estimate of the mean of (3.9) by averaging the noise samples. The accuracy of the noise estimate allows us to precisely set a threshold based on a desired false alarm rate. Here, we choose to minimize the probability of missed detection in order to limit the bias on the channel estimate, so we choose a relatively high probability of false alarm of 5×10^{-3}. The detection threshold that achieves this probability of false alarm is

$$\gamma_{\mathrm{c}} = \mu \widehat{\sigma}_{\mathrm{w}}^2, \tag{3.14}$$

where μ is dependent on the number of preamble symbols used for the power delay profile estimate. The scale factor can be obtained by solving the following equation, where $P(\psi_{\mathrm{k}}, \alpha, \Theta)$ is the PDF of the noise variance estimate defined in (3.9), for an arbitrary receiver configuration by finding the value of μ that satisfies

$$5 \times 10^{-3} = \int_{\mu}^{\infty} P(\psi_{\mathrm{k}}, \alpha, \Theta) d\psi_{\mathrm{k}}. \tag{3.15}$$

The decisions made based on this threshold can be expressed as

$$\begin{aligned} H_0 &: \widehat{S}_n < \gamma_{\mathrm{c}} \\ H_1 &: \widehat{S}_n \geq \gamma_{\mathrm{c}}. \end{aligned} \tag{3.16}$$

To reduce the effects of the high false alarm rate given by the threshold in (3.14), we add a second step to the channel delay spread estimator. This step takes advantage of the

fact that false detections are uniformly distributed across the vector $\widehat{\mathbf{S}}$, while valid channel samples will likely be clustered closely together. Therefore, a sliding window can be used to identify PDP samples that belong to a cluster of valid channel samples and identify lone samples that are likely due to a false detection. The size of the window, W, can be chosen based on some prior knowledge about the wireless environment, or it can be chosen based on a desired lower probability of false alarm.

Within the sliding window, we model the probability of false detection at each sample index with a Bernoulli distribution and denote p as the probability of false alarm given by the threshold in (3.14). Because we reject lone samples that surpass the detection threshold within the window, the new false alarm rate is the probability of more than one false detection within the window. This can be computed as

$$P_{\text{FA,window}} = \sum_{n=2}^{W} \binom{W}{n} p^n (1-p)^{W-n}. \tag{3.17}$$

For a numeric example of the improvement in performance gained from the window-based false alarm reduction technique, we start with the threshold in (3.14) that has a corresponding probability of false alarm of 5×10^{-3}. If a window size of $W = 8$ is selected, the probability of false alarm is reduced to 6.9×10^{-4}.

To link all of the work developed in the thesis together, we add the interference rejection and channel length detection algorithms to Fig. 2.2 for a block diagram of the full design in Fig. 3.6. In Fig. 3.6, the analysis filter bank output is passed to the noise estimation algorithm, which identifies interference in accordance with the process in Section 3.2 and passes the interference locations to an interpolation algorithm. Additionally, the channel noise estimate is passed to the channel length detection algorithm, which provides an estimate of L_{c} to the denoising flat-gain estimation algorithm. With these additional components in the design, performance near to the CRLB can be obtained.

3.4 Simulation Results

To validate the theory developed in the previous sections, the channel length detection algorithm was evaluated in several Monte Carlo simulations. All simulations were run with the following configuration:

- Filter Bank Upsampling Rate (L) = 512.

- Number of Active Subcarriers (N) = 256.
- Periodic Pilot Sequence Length (K) = 32.
- The channel is static over the duration of the FBMC-SS Packet.
- Pilot symbols ($a(n)$) are transmitted on all subcarriers during the preamble.
- Perfect timing synchronization and carrier synchronization are assumed.
- The transient introduced by the channel is absorbed by the beginning of the preamble during packet detection such that the channel estimate is performed on non-transient data.
- No interference is present in the signal band.
- The channel length detection algorithm proposed in [38] was configured for a probability of error (P_e) of 1×10^{-6}.

3.4.1 Simulation Results for a Short Channel Response

The first test evaluates the channel length detection algorithm for a short multipath channel similar to Fig. 2.3. In this scenario, the channel length detection algorithm can accurately identify valid channel impulse response samples in very low SNR environments. This can be attributed to the fact that the channel samples are relatively closely spaced together and have similar path gains. As a result of this accurate channel identification, the denoising algorithm can be adjusted for near-CRLB performance.

The performance of the flat-gain channel estimator with the channel length detection algorithm was compared to several alternative methods. The first alternative is the current channel estimation implementation, which forms a channel estimate using (2.9) and does not perform denoising. We refer to this algorithm as the "sample mean estimator" in the results. The second alternative is the flat-gain channel estimator with channel length detection given by [38]. The results corresponding to this method are labeled as "flat-gain estimator with Zhu et al. channel length detection". In these results, it will be shown that the combination of the channel length detection and flat-gain channel estimation methods presented in this thesis provide better performance than the alternatives in low SNR environments.

We measured several parameters to validate the theory developed for the channel length detection algorithm. The first result we examine is the false alarm rate of the channel length detection algorithm proposed in the thesis. For this configuration, the probability of false alarm in the channel length detection algorithm was achieved by setting μ in (3.14) to 1.76. The measured simulation results are shown in Fig. 3.7. It is evident that the results closely match theory, with a constant measured probability of false alarm of 6×10^{-3} measured in relation to the expected value of 5×10^{-3}. Additionally, the false alarm rate after windowing, shown in red, is close to the expected value of 6.9×10^{-4}.

The proposed algorithm's performance is quantified by the bias of the channel estimator, which indicates how many channel impulse response samples were wrongfully removed by the denoising operation. The bias of the flat-gain channel estimator with the channel length estimation algorithm proposed in this thesis is shown in blue in Fig. 3.8. Additionally, the bias is evaluated in relation to the channel length detection algorithm proposed in [38]. It is evident that the algorithm proposed in this thesis has a more accurate threshold that results in less bias in the channel estimate at low SNR levels.

Additionally, the overall NMSE performance of the estimation algorithms were evaluated relative to the CRLB computed in Section 2.4. The NMSE metric evaluates how accurate the channel estimate is, and encompasses both the estimation bias and the amount of noise in the estimate. The simulated NMSE results between the three channel estimation schemes are presented in Fig. 3.9. The flat-gain estimator with channel length detection from [38] is shown in yellow, and the NMSE follows a similar pattern to Fig. 3.8 due to the large bias caused by the removal of valid channel samples. It is evident that the bias significantly degraded the performance of the estimator and offset any benefits from the noise removal. On the other hand, the flat-gain estimator with the joint noise estimation (in red) and channel length detection algorithm presented in this thesis performed near the CRLB. Based on these results, the denoising estimator with channel detection achieves superior performance to the current estimation algorithm and also outperforms an alternative method in the literature at low signal to noise ratios.

Lastly, the bit-error rate (BER) performance was evaluated between the different algorithms in Fig. 3.10. These results provide similar conclusions to the NMSE measurements, where the accurate channel length measurement provided by the thesis (red line) allowed

the receiver to meet the theoretical BER performance for BPSK modulation (dashed magenta line). The alternative method (yellow line) suffered from an approximately 0.5 dB implementation loss due to estimator bias.

3.4.2 Simulation Results for a Long Channel Response

The purpose of this subsection is to evaluate the channel length detection algorithm on the longer channel response in Fig. 3.5. In this test case, a subset of the channel impulse response samples were wrapped around to the end of the vector to emulate the effects of the FBMC-SS timing acquisition process. The purpose of this is to illustrate the benefits of coupling the channel estimate denoising process with a channel length detection scheme to prevent bias. The BER performance of the FBMC-SS receiver is used to measure the impact of detecting wrapping channel impulse response samples. These results are provided in Fig. 3.11.

In Fig. 3.11, we evaluated three different algorithms. The first algorithm is the Flat-gain ML estimator (blue line) that assumes the channel length is $N/2$ samples long, or approximately 4 μs long in time. This is meant to emulate a conservative receiver configuration that has no *a priori* knowledge of the channel impulse response length, but wishes to remove noise without biasing the estimate. However, for this conservative configuration, the channel length assumption does not account for any wrapping in the channel samples. The second algorithm (red line) is the FBMC-SS receiver with the Flat-gain channel estimator and the channel length detection algorithm proposed in this thesis. The third algorithm (yellow line) utilizes the channel length detection algorithm proposed in [38]. It is evident from the results that the bias introduced by removing channel samples that wrapped to the end of the vector caused significant performance degradation for the first case. However, with both channel length detection algorithms, the loss in performance was mitigated by detecting the wrap-around - with the channel length detection algorithm presented in this thesis slightly outperforming the alternative from the literature.

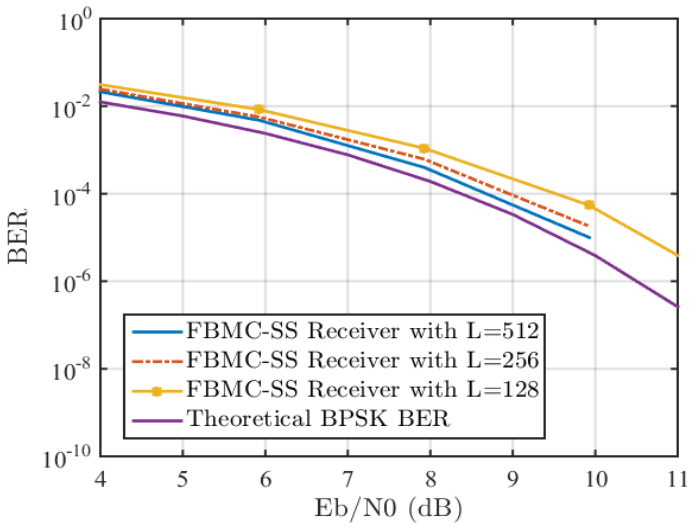

Figure 3.1. BER performance test for the coherence bandwidth constraint with an LTE EVA channel

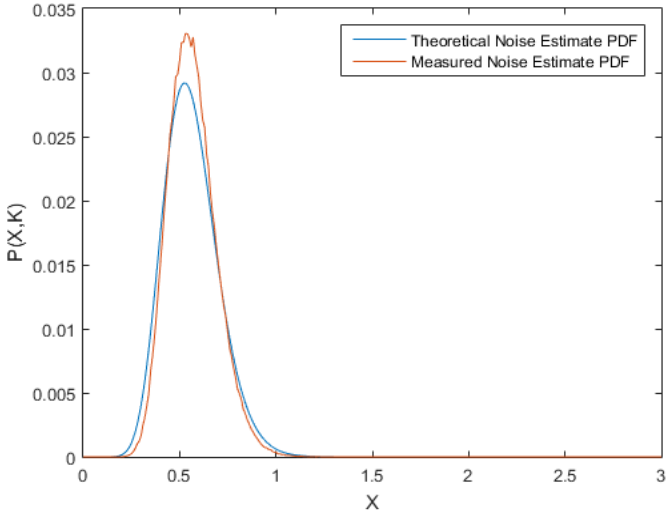

Figure 3.2. Theoretical PDF of the noise variance estimate vs. measured PDF of noise variance estimate in a white noise channel with an SNR (Es/No) of 0 dB

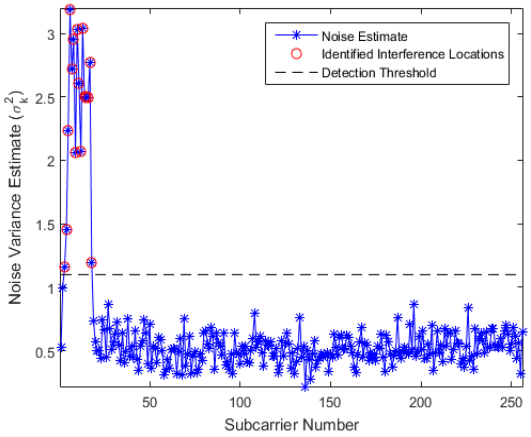

Figure 3.3. Interference identification with the noise variance estimate

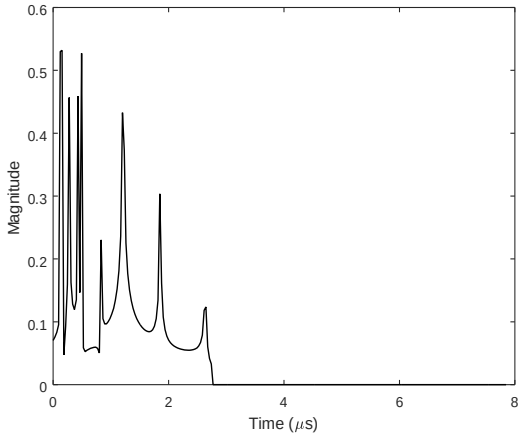

Figure 3.4. Example Rayleigh multipath channel impulse response

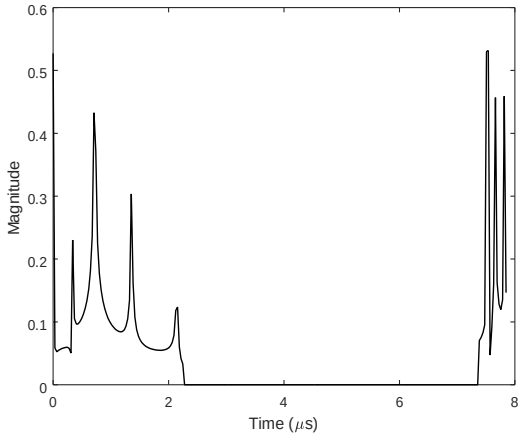

Figure 3.5. Circularly shifted Rayleigh multipath channel response after timing acquisition in the FBMC-SS receiver

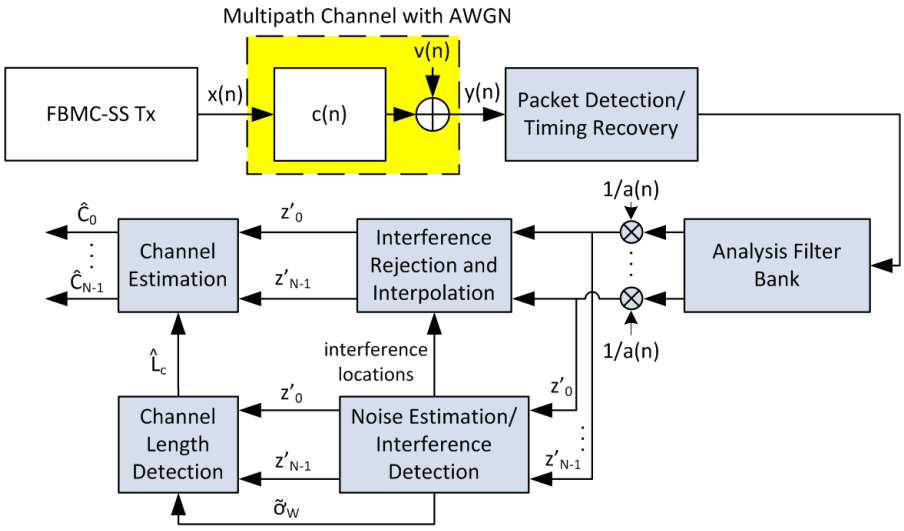

Figure 3.6. System model for the full flat-gain channel estimator

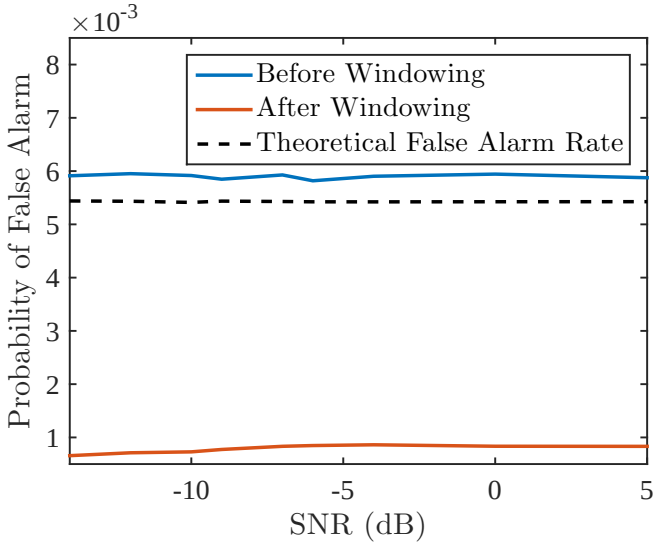

Figure 3.7. Channel length detection (CLD) probability of false alarm simulation

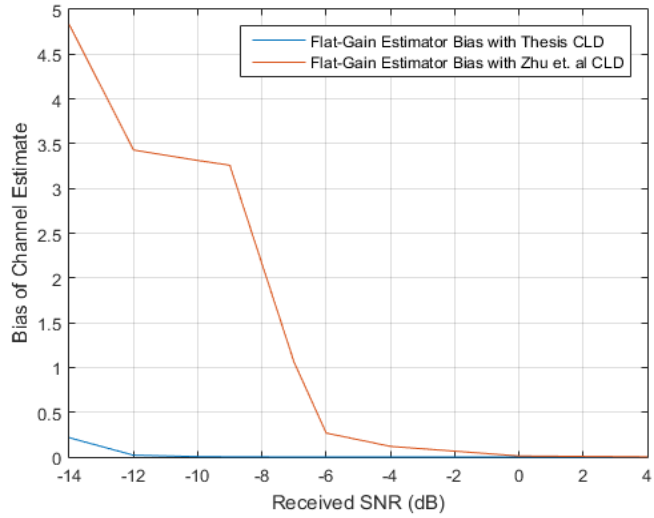

Figure 3.8. Bias of the channel estimate with CLD for a short multipath channel

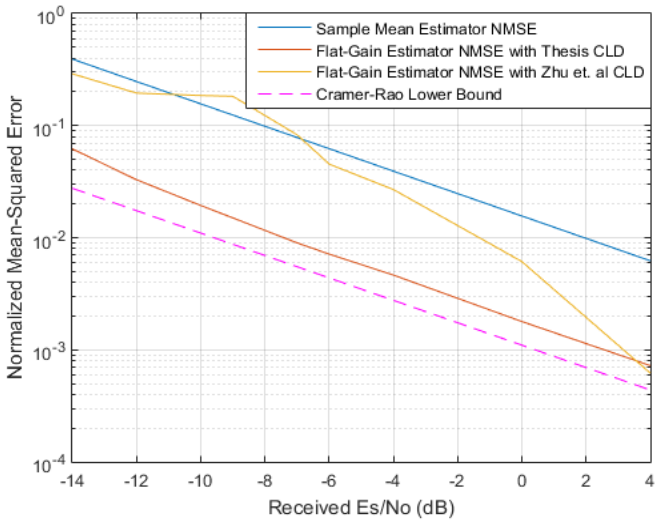

Figure 3.9. Normalized MSE of the channel estimate with CLD for a short multipath channel

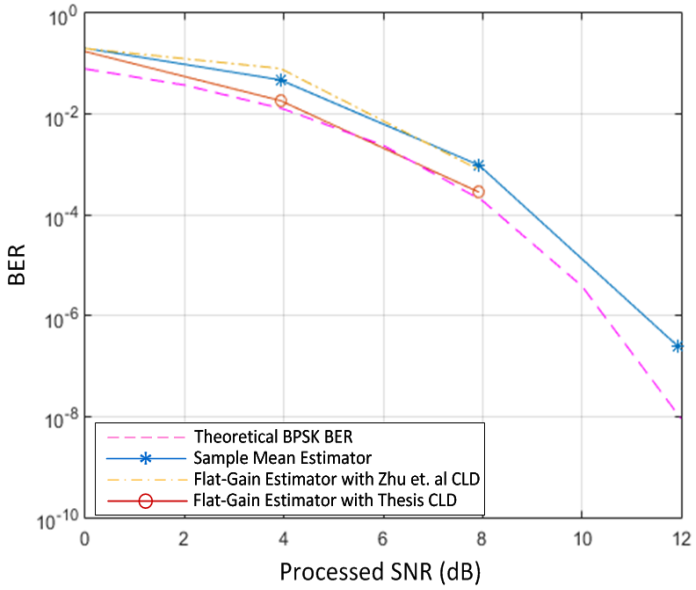

Figure 3.10. BER performance assessment of the flat-gain estimator with CLD for a short multipath channel

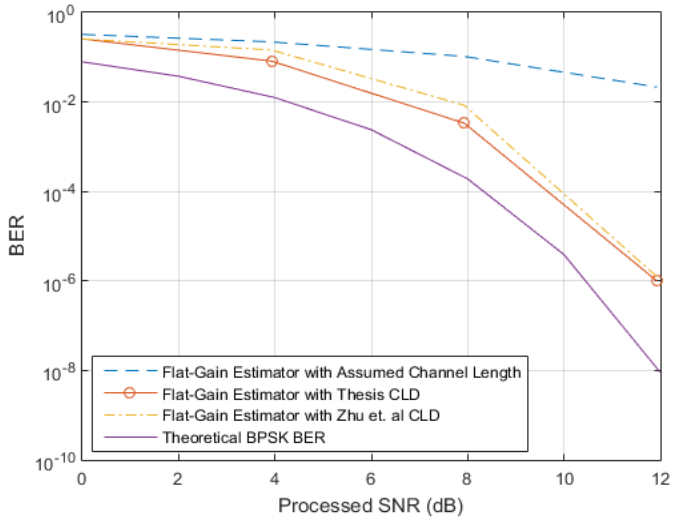

Figure 3.11. BER performance assessment of the flat-gain estimator with CLD for a long multipath channel with wrapping

CHAPTER 4

CONCLUSION

In this thesis, we presented two maximum likelihood channel estimation schemes for FBMC-SS and evaluated their performance against their respective Cramer-Rao Lower Bounds. An OFDM-like channel estimator was derived that utilizes the tones generated by a periodic pilot sequence to estimate the channel frequency response, and it was shown through analysis that this estimator meets the CRLB with perfect knowledge of the channel impulse response duration. A standard alternative channel estimation method, denoted as the flat-gain channel estimator, was analyzed and shown to also meet the CRLB when the assumptions surrounding the formulation of the estimator are accurate. We provided simulation results which show the flat-gain channel estimator only meets the CRLB for relatively time-limited channels at lower SNR levels. On the other hand, the simulation results confirmed that the OFDM-like channel estimator meets the CRLB for channels with either a short time duration or high frequency selectivity, regardless of the SNR. We also provided details regarding the implementation of these two algorithms, and showed that the OFDM-like channel estimator can be implemented more efficiently than the flat-gain channel estimator under the assumption that the channel noise is flat across the received frequency bands.

Next, we pursued the practical implementation of the flat-gain channel estimator by investigating interference rejection and channel length detection. A simple CFAR thresholding method was proposed to identify subcarriers that contain significant interference, and rejecting these subcarriers allows us to make a good assumption that the noise in the channel estimate is approximately white and Gaussian. After rejecting colored noise (interference), the proposed channel length detection algorithm utilizes the noise variance estimate to accurately identify time indexes that contain channel samples and maximizes the ability of the denoising operation in the flat-gain estimator to remove noise without biasing the result.

It was demonstrated that for a short channel length, the channel length detection algorithm could be used to achieve performance near the CRLB. For longer channel responses, the algorithm is an effective method for reducing bias when the FBMC-SS timing recovery algorithm causes channel samples to circularly shift.

REFERENCES

[1] B. Farhang-Boroujeny, "OFDM Versus Filter Bank Multicarrier," *IEEE Signal Process. Mag.*, vol. 28, no. 3, pp. 92–112, 2011.

[2] D. Wasden, H. Moradi, and B. Farhang-Boroujeny, "Design and Implementation of an Underlay Control Channel for Cognitive Radios," *IEEE J. Sel. Areas Commun.*, vol. 30, no. 10, pp. 1875–1889, 2012.

[3] M. Morelli and U. Mengali, "A Comparison of Pilot-Aided Channel Estimation Methods for OFDM Systems," *IEEE Trans. Acoust., Speech, Signal Process.*, vol. 49, no. 12, pp. 3065–3073, 2001.

[4] J.-p. Javaudin, D. Lacroix, and A. Rouxel, "Pilot-Aided Channel Estimation for OFDM / OQAM," in *Proc. IEEE. Veh. Tech. Conf.*, 2003, pp. 1581–1585.

[5] D. Kong, D. Qu, and T. Jiang, "Time Domain Channel Estimation for OQAM-OFDM Systems: Algorithms and Performance Bounds," *IEEE Trans. Signal Process.*, vol. 62, no. 2, pp. 322–330, 2014.

[6] Y. Zhao and A. Huang, "A Novel Channel Estimation Method for OFDM Mobile Communication Systems Based on Pilot Signals and Transform-Domain Processing," in *Veh. Technol. Conf. 1997, IEEE 47th*, 1997, pp. 2089–2093.

[7] M. Sandell and S. K. Wilson, "On Channel Estimation in OFDM Systems," in *IEEE Veh. Tech. Conf.*, no. 1, 1995, pp. 815–819.

[8] H. Minn, S. Member, and V. K. Bhargava, "An Investigation into Time-Domain Approach for OFDM Channel Estimation," *IEEE Trans. Broadcast.*, vol. 46, no. 4, pp. 240–248, 2000.

[9] T. Fusco, E. Member, A. Petrella, and M. Tanda, "Joint Symbol Timing and CFO Estimation for OFDM / OQAM Systems in Multipath Channels," *EURASIP J. Adv. Signal Process.*, vol. 2010, pp. 1120–1124, 2010.

[10] P. Amini and B. Farhang-Boroujeny, "Packet Format Design and Decision Directed Tracking Methods for Filter Bank Multicarrier Systems," *EURASIP J. Appl. Signal Processing*, vol. vol. 2010, no. doi:10.1155/2010/307983, 2010.

[11] Hamid Saeedi-Sourck, Saeed Sadri, Yan Wu and B. Farhang-Boroujeny, "Near Maximum Likelihood Synchronization for Filter Bank Multicarrier Systems," *IEEE Wirel. Commun. Lett.*, vol. 2, no. 2, pp. 235–238, 2013.

[12] E. Kofidis, "Short Preamble-Based Estimation of Highly Frequency Selective Channels in FBMC/OQAM," *Proc. IEEE Int. Conf. Acoust, Speech, Signal Proc.*, pp. 8058–8062, 2014.

[13] ——, "Preamble-based Estimation of Highly Frequency Selective Channels in MIMO-FBMC/OQAM Systems," *Proc. Eur. Wirel. Conf.*, pp. 166–171, 2015.

[14] E. Kofidis, D. Katselis, A. Rontogiannis and S. Theodoridi, "Preamble-Based Channel Estimation in OFDM/OQAM Systems: A Review," *Signal Processing*, vol. 93, no. 7, pp. 2038–2054, 2013.

[15] L. G. Baltar, A. Mezghani, and J. A. Nossek, "Spectral Efficient Channel Estimation Algorithms for FBMC / OQAM Systems : A Comparison," in *11th Int. Symp. Wirel. Commun. Syst.*, 2014, pp. 707–711.

[16] L. G. Baltar, M. Newinger, and J. A. Nossek, "Structured Subchannel Impulse Response Estimation for Filter Bank Based Multicarrier Systems," *Proc. Int. Symp. Wirel. Commun. Syst.*, pp. 191–195, 2012.

[17] T. Haddadin, S. A. Laraway, A. Majid, T. Sibbett, D. L. Wasden, B. F. Lo, L. Landon, D. Couch, H. Moradi, and B. Farhang-Boroujeny, "An Underlay Communication Channel for 5G Cognitive Mesh Networks: Packet Design, Implementation, Analysis, and Experimental Results," *2016 IEEE Int. Conf. Commun. Work. ICC 2016*, pp. 498–504, 2016.

[18] Taylor Sibbett, Hussein Moradi and B. Farhang-Boroujeny, "Novel Maximum-based Timing Acquisition for Spread-Spectrum Communications," in *GC16 Work. ET5G*, 2016.

[19] J. Driggs, T. Sibbett, H. Moradi, and B. Farhang-boroujeny, "Channel Estimation for Filter Bank Multicarrier Systems in Low SNR Environments," in *IEEE ICC 2017*. Paris: IEEE, 2017.

[20] J. Driggs, H. Moradi, and B. Farhang-Boroujeny, "A Joint Noise Variance and Channel Delay Spread Estimation Algorithm for Low SNR/Contested Environments," *Under Prep.*, 2018.

[21] S. M. Kay, *Fundamentals of Statistical Signal Processing: Estimation Theory*. Upper Saddle River, NJ: Prentice-Hall, Inc., 1993.

[22] T. Specification, "Etsi ts 136 104," *(3GPP TS 36.101 version 10.3.0 Release 10*, vol. 0, 2011.

[23] Report ITU-R M.2135-1, "Guidelines for Evaluation of Radio Interface Technologies for IMT Advanced," *Evaluation*, vol. 93, no. 3, 2009. [Online]. Available: http://www.ncbi.nlm.nih.gov/pubmed/19923880

[24] P. Ö. Henrik Asplund, Kjell Larsson, "How Typical is the "Typical Urban" Channel Model?" in *IEEE Veh. Tech. Conf.*, 2008, pp. 340–343.

[25] B. Farhang-Boroujeny and S. Gazor, "Generalized Sliding FFT and Its Application to Implementation of Block LMS Adaptive Filters," *IEEE Trans. Signal Process.*, vol. 42, no. 3, pp. 532–538, 1994.

[26] J. D. Markel, "FFT Pruning," *IEEE Trans. Audio Electroacoust.*, vol. AU-19, no. 4, pp. 305–311, 1971.

[27] A. Goldsmith, *Wireless Communications*, i ed. New York, NY: Cambridge University Press, 2005.

[28] W. Lee, *Mobile Cellular Telecommunications Systems*. New York, NY: McGraw Hill, 1989.

[29] S. Haykin, "Cognitive Radio: Brain-empowered Wireless Communications," *IEEE J. Sel. Areas Commun.*, vol. 23, no. 2, pp. 201–220, 2005.

[30] X. Zheng, L. Cui, J. Chen, Q. Wu, and J. Wang, "Cooperative Spectrum Sensing in Cognitive Radio Systems," *2008 Congr. Image Signal Process.*, no. 2007, pp. 262–266, 2008. [Online]. Available: http://ieeexplore.ieee.org/lpdocs/epic03/wrapper.htm?arnumber=4566829

[31] B. Farhang-Boroujeny and R. Kempter, "Multicarrier Communication Techniques for Spectrum Sensing and Communication in Cognitive Radios," *IEEE Commun. Mag.*, vol. 46, no. 4, pp. 80–85, 2008.

[32] B. Farhang-Boroujeny, "Filter Bank Spectrum Sensing for Cognitive Radios," *IEEE Trans. Signal Process.*, vol. 56, no. 5, pp. 1801–1811, 2008.

[33] S. M. Kay, *Fundamentals of Statistical Signal Processing: Detection Theory*. Upper Saddle River, NJ: Prentice-Hall, Inc., 1993.

[34] R. Tandra and A. Sahai, "Walls for Signal Detection," *Sel. Top. Signal Process. IEEE J.*, vol. 2, no. 1, pp. 4–17, 2008. [Online]. Available: http://ieeexplore.ieee.org/xpl/articleDetails.jsp?arnumber=4453895

[35] O. Simeone, Y. Bar-Ness, and U. Spagnolini, "Pilot-based Channel Estimation for OFDM Systems by Tracking the Delay Subspace," *IEEE Trans. Wirel. Commun.*, vol. 3, no. 1, pp. 315–325, 2004.

[36] M. Li, J. Tan, and W. Zhang, "A Channel Estimation Method Based on Frequency-Domain Pilots and Time-Domain Processing for OFDM Systems," *IEEE Trans. Consum. Electron.*, vol. 50, no. 4, pp. 1049–1057, 2004.

[37] P. P. Data, "(12) Ulllted States Patent," 2011.

[38] M. Zhu, A. B. Awoseyila, and B. G. Evans, "Low Complexity Time-domain Channel and Delay Spread Estimation for OFDM Systems," *IEEE Trans. Consum. Electron.*, vol. 56, no. 4, pp. 2170–2177, 2010.

[39] T. Cui and C. Tellambura, "Power Delay Profile and Noise Variance Estimation for OFDM," *IEEE Commun. Lett.*, vol. 10, no. 1, pp. 25–27, 2006.

[40] B. Yang, K. B. Letaief, and R. S. Cheng, "Timing Recovery for OFDM Transmission," *IEEE J. Sel. Areas Commun.*, vol. 18, no. 11, pp. 2278–2291, 2000.